Adaptive ferroelectric states in KNN-based piezoceramics: Unveiling the mechanism of enhancing piezoelectric properties through multiple phase boundary engineering

Yang Liu [a,b,1], Jinhui Fan [a,1], Xudong Qi [c,*], Bingzhong Shen [a], Rui Zhang [a,*], Kui Yao [b,*]

[a] School of Instrumentation Science and Engineering, Harbin Institute of Technology, Harbin 150080, China
[b] Institute of Materials Research and Engineering (IMRE), A*STAR (Agency for Science, Technology and Research), Singapore 138634, Singapore
[c] School of Physics and Electronic Engineering, Key Laboratory for Photonic and Electronic Bandgap Materials, Ministry of Education, Harbin Normal University, Harbin 150025, China

ARTICLE INFO

Keywords:
KNN ceramics
Lead-free
Phase boundaries
Piezoelectric performances

ABSTRACT

Developing high-performance lead-free piezoceramics, such as $(K,Na)NbO_3$ (KNN) material, is critical to achieving environmental sustainability in next-generation electromechanical devices. Although substantial advancements have been made in KNN-based ceramics, a general coherent framework is lacking that links microscopic structure to the enhancement of macroscopic properties. Our findings indicate that the enhanced performance of KNN-based ceramics in multiphase coexistence boundaries can be attributed to the formation of self-adjusting nanodomains in response to strong local structural heterogeneity. The self-adjusting behavior of domain structure is an outcome of minimizing the local stress generated by the lattice mismatch within KNN-based ceramics, which conforms to the thermodynamic principles that favor minimizing total free energy. Guided by this strategy, the present work achieves a significant improvement of electromechanical properties, including a piezoelectric coefficient (d_{33}) of ~585 pC N^{-1}, an electromechanical coupling factor (k_p) of ~62 %, and a figure of merit ($d_{33} \times g_{33}$) of ~12.78 $\times 10^{-12}$ m^2 N^{-1}. This study offers a new strategy for developing lead-free piezoceramics through dedicated design of novel phase boundaries.

1. Introduction

Piezoceramic materials are essential for electromechanical conversion in various devices including actuators, sensors, ultrasonic transducers, and energy harvesters [1–3]. Since the 1960s, $Pb(Zr,Ti)O_3$ (PZT)-based ceramics have been the primary choice in the commercial piezoceramics market because of their superior piezoelectric properties and well established massive manufacturing process [4,5]. However, the environmental and health risks associated with their toxic lead content, exceeding 60 % by weight, have prompted intensive research efforts into lead-free alternatives [6,7]. Among lead-free piezoceramics including $BaTiO_3$ (BT), $BiFeO_3$ (BFO), $(Bi,Na)TiO_3$ (BNT), and $(K,Na)NbO_3$ (KNN) ceramics, KNN ceramics are regarded as a promising lead-free option despite inferior to PZT in terms of electromechanical performance [8–12].

Over the past two decades, strategies to enhance the electromechanical properties of KNN ceramics have included advanced sintering techniques, A/B-site doping, multilayer approaches, polar nanoregions (PNRs) and polymorphic phase boundaries (PPB) [13–19]. In 2004, a work from Saito et al. significantly enhanced the performance of KNN ceramics by structural texturing and the construction of orthorhombic-tetragonal (O-T) phase boundaries, achieving a piezoelectric coefficient (d_{33}) of ~416 pC N^{-1} and improved temperature stability [11]. In 2014, Wu et al. developed KNN ceramics with a d_{33} of ~490 pC N^{-1} by creating a rhombohedral-tetragonal (R-T) phase structure [12]. Similarly, Li et al. used lattice softening and reduced distortion within R-T structure to achieve a d_{33} of ~500 pC N^{-1} and an electromechanical coupling factor (k_p) of ~54 % [20]. Through the construction of PPB, significant progress has been made in improving the electromechanical properties of KNN-based ceramics.

Recently, the strategy of constructing tricritical phase (R-O-T) coexistence, has emerged as a groundbreaking strategy to enhance the electromechanical properties of KNN-based ceramics [21]. Tao et al. achieved a d_{33} of ~650 pC N^{-1} with a composition of (K,Na)NbSbO_3-Bi(Na,K)ZrO_3-Fe_2O_3-AgSbO_3 (KNNS-BNKZ-Fe-AS) by engineering this novel phase boundary (NPB), a specific subclass of PPB [22]. The concept of NPB, especially its realization through R-O-T phase coexistence, is not well accepted and has generated considerable debate due to its complexity and lack of solid understanding of its underlying mechanisms. The superior performance of ceramics with PPB is thought to result from a combination of many co-related factors, including a flattened energy landscape, local structural heterogeneity, complex domain configuration, and low polarization anisotropy [23–26]. Despite these advances, the field still lacks a coherent framework to explain how these microscopic characteristics affect the enhancement of macroscopic properties.

In this work, the typical 0.96 $K_{0.48}Na_{0.52}Nb_{0.96}Sb_{0.04}O_3-0.04Bi_{0.5}Na_{0.5}ZrO_3$ ceramic of PPB is selected as the research subject [27]. The incorporation of $BaZrO_3$ regulates the formation of R-O-T phase coexistence in samples, hereinafter referred to as KNN-BZ ceramics. The electromechanical properties of $d_{33} \sim 585$ pC N^{-1} and $k_p \sim$ 62 % are obtained in KNN-BZ ceramics. Our research describes the interplay between structure and performance, revealing the complex relationships among factors driving the high performance. This study

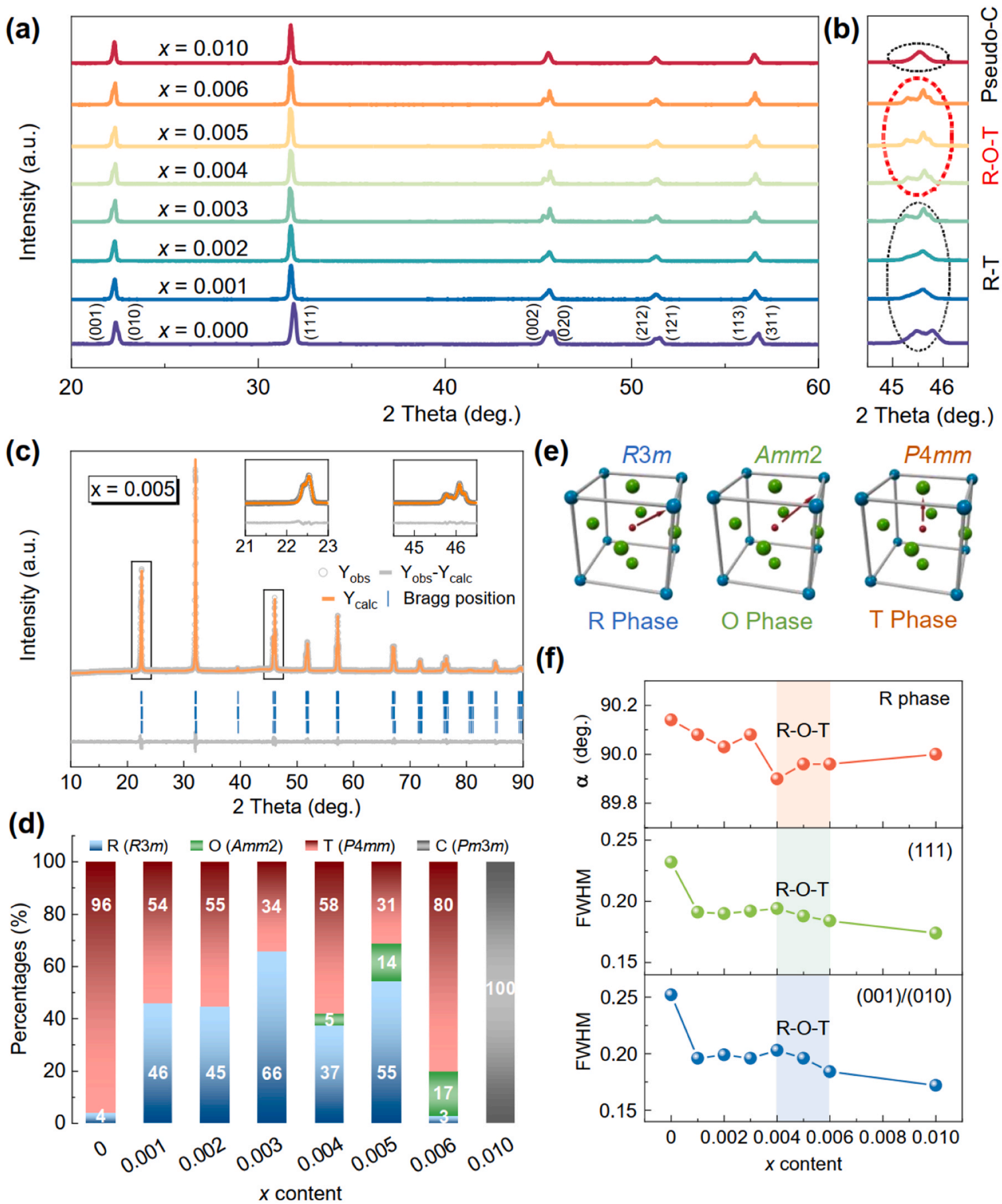

Fig. 1. (a) XRD patterns of KNN-BZ ceramics. (b) Expanded XRD patterns with $2\theta = 44.5^\circ \sim 46.5^\circ$. (c) Rietveld refinement of the ceramic with $x = 0.005$. (d) Phase percentages of KNN-BZ ceramics. (e) Schematic of various lattice structures and the corresponding polarization orientation. (f) α angle of R phase and FWHM for the (111) and (001)/(010) diffraction peaks with variations of the BZ content.

offers an insight for supporting the development of lead-free piezoceramics from the perspective of phase boundary engineering.

2. Results and discussion

2.1. Crystal structure

To reveal the phase structure of KNN-BZ ceramics, X-ray diffraction (XRD) patterns are shown in Fig. 1a. The KNN-BZ ceramics with a dense grain microstructure (Figure S1-S2) exhibit pure perovskite structure without second phase, demonstrating the effective incorporation of BZ into the KNN matrix. The $\{200\}_{pc}$ diffraction peak around 45° is crucial for identifying the phase structure of perovskite ferroelectrics, as shown in Fig. 1b. For a pure R phase (space group: *R3m*) structure, a single $\{200\}_{pc}$ peak can be observed. As for a pure O phase (space group: *Amm*2) structure, the intensity of the $(002)_{pc}$ peak exhibits twice that of

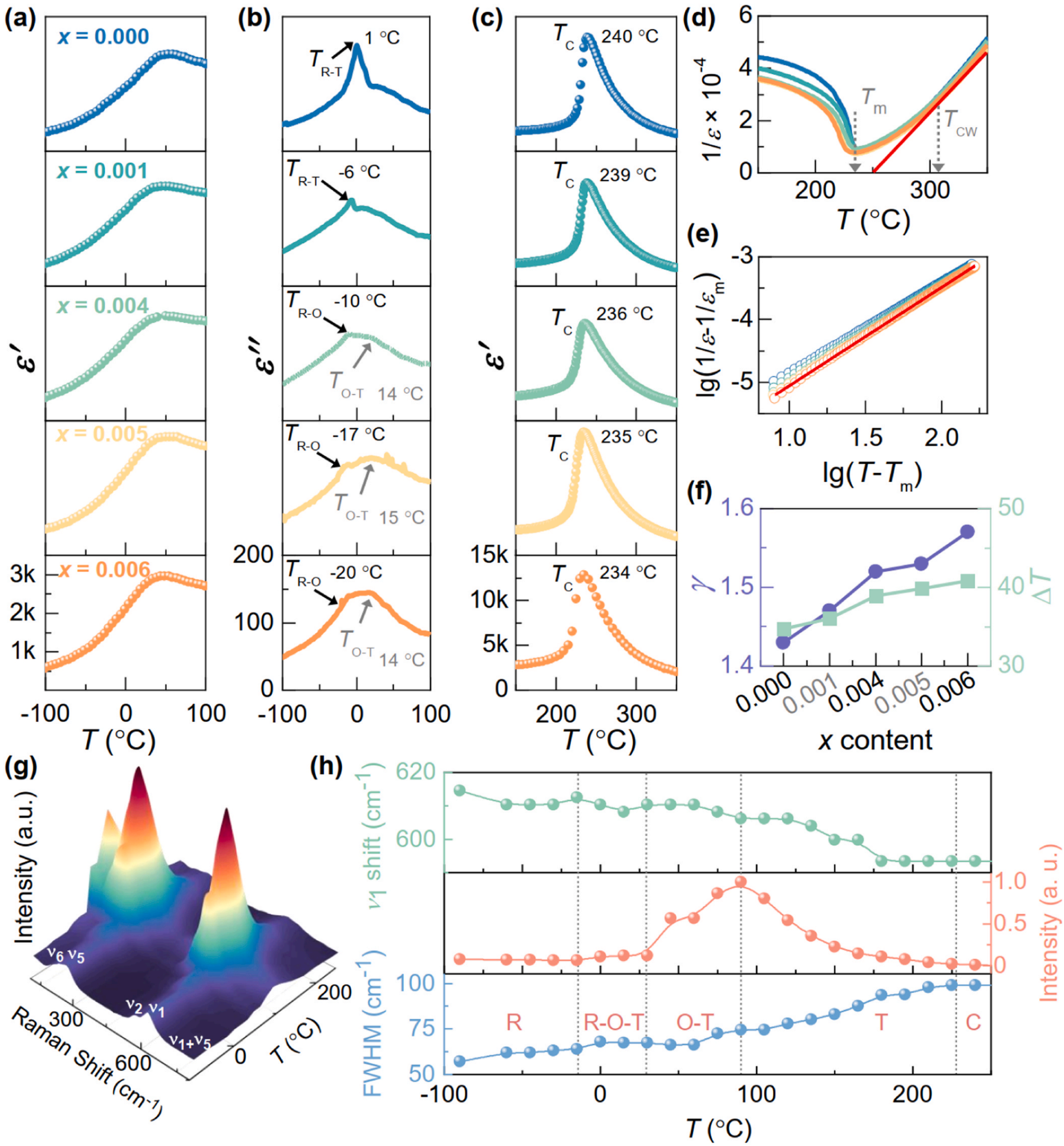

Fig. 2. (a-b) ε'-T and ε''-T curves of KNN-BZ ceramics measured over the temperature range of −100 °C to 100 °C. (c) ε'-T curves of KNN-BZ ceramics measured from 150 °C to 350 °C. (d) Relationship between T and $1/\varepsilon\times10^{-4}$. (e) Linear fitting between lg(T-T_m) and lg($1/\varepsilon$-$1/\varepsilon_m$). (f) Comparison of γ and $\triangle T$ with varying x content. (g) Temperature dependence of Raman spectra for the ceramic with x = 0.005. (h) FWHM, peak shift, and intensity of $\nu1$ mode as a function of temperature for the ceramic with x = 0.005.

the $(020)_{pc}$ peak, while for a pure T phase (space group: *P4mm*) structure both peaks exhibit opposite patterns [28]. In the present cases, the deviation in the relative intensity ratio of peaks around 45° from the established norm indicates the presence of multiphase coexistence within the KNN-BZ ceramics. The results from XRD Rietveld refinement of the ceramic with $x = 0.005$ (Fig. 1c) indicate that the diffraction peaks can be well fitted with the R-O-T phase, with an error factor of R_p (3.70). The Rietveld refinement results for other KNN-BZ ceramics are displayed in Figure S3-S10.

In Fig. 1d, it is observed that the ceramic with $x = 0.000$ exhibits a multiphase state, characterized by the R-T coexistence phase, with a dominant T phase. As the BZ content increases to $x = 0.001$, there is a marked increase in the proportion of the R phase. For ceramics with $x = 0.004 \sim 0.006$, the structure transitions to a complex R-O-T phase, with an increasing proportion of the O phase. The schematic of various lattice structures and the corresponding polarization orientation of R, O, and T phase structures are shown in Fig. 1e. The evolution of phase structure can be attributed to ionic substitutions of Ba^{2+} for original A-site cations and Zr^{4+} for original B-site cations. This substitution is driven by differences between the introduced additives and the original ions in terms of ionic size, valence, and electronegativity. Similar phenomena have been reported in several studies concerning KNN-based ceramics [29, 30]. Fig. 1f shows the evolution of α angle in the R phase and the full width at half maximum (FWHM) of (111) and (001)/(010) diffraction peaks, further confirming the phase transition process in KNN-BZ ceramics.

2.2. Dielectric property

Analyzing the temperature dependence of dielectric constant (ε'-T) is an effective method to identify the phase transition process of KNN-based ceramics. In Fig. 2a, all ε'-T curves exhibit a single dielectric anomaly between −100 °C and 100 °C, corresponding to the ferroelectric-ferroelectric phase transition. To further obtain phase transition information within KNN-BZ ceramics, the temperature dependence imaginary part of dielectric constants (ε''-T) is shown in Fig. 2b. For ceramics with $x = 0.004 \sim 0.006$, $T_{R\text{-}O}$ and $T_{O\text{-}T}$ transition temperatures identified by abnormal peaks in the ε''-T curves, are −10 °C, −17 °C, −20 °C and 14 °C, 15 °C, 14 °C, respectively. The increasing temperature difference from $T_{R\text{-}O}$ to $T_{O\text{-}T}$ indicates that the O phase in the matrix gradually increases, which is consistent with results from the refined XRD data. The dielectric anomaly observed in the ε'-T curves at higher temperature corresponds to the ferroelectric-paraelectric phase transition at Curie temperature (T_C), as shown in Fig. 2c and Figure S11. Moreover, the increase of BZ content has no obvious effect on T_C, thus ensuring the practicability of KNN-BZ ceramics in applications.

The analysis of ε'-T curves for KNN-BZ ceramics shows that there is an obvious diffuse phase transition (DPT) around T_C. This observation indicates an inherent structural heterogeneity in the samples that distinguishes them from normal perovskite ferroelectrics. As shown in Fig. 2d-e, the structure heterogeneity hinders the obey of DPT-type ferroelectrics to the Curie-Weiss law (Equation S1). The offset represented by ΔT (Equation S2) denotes the DPT behavior [31]. A modified Curie-Weiss law (Equation S3) is employed to show a linear fitting of the inverse dielectric constant ($1/\varepsilon$)-temperature spectra above T_m (the temperature where the ε reaches the maximum) [32]. Within this framework, the larger slope (γ) value, the stronger DPT behavior. Fig. 2f shows that both γ and ΔT increase as a function of BZ content, suggesting that the increase of BZ content enhances the DPT behavior induced by strong structural heterogeneity [33]. To further confirm the complexity of phase transitions in R-O-T phase samples, temperature dependence Raman spectra are utilized. In Fig. 2g-h, the anomalies observed in ceramic with $x = 0.005$ near −15 °C and 30 °C confirm the occurrence of R-O and O-T phase transitions. The above results show that by regulating the BZ content, a “new phase boundary (NPB)” with x values ranging from 0.004 to 0.006 is found in KNN-BZ ceramics, which is characterized by the R-O-T phase coexistence.

2.3. Macroscopic electromechanical property

Fig. 3a shows the polarization-electric field (*P-E*) hysteresis loop and current-electric field (*J-E*) curve of KNN-BZ ceramics. The sample exhibits a saturated *P-E* loop with a high rectangularity degree, whereas the *J-E* curve presents a double current peak at coercive fields (E_C), which is caused by an electric field driven polarization switching process [34]. In Fig. 3b, under different BZ content, maximum polarization (P_{max}) remains relatively constant. In contrast, in the samples with NPB, remnant polarization (P_r) maintains a high value, peaking at $x = 0.005$, while E_C decreases slightly upon the introduction of BZ content. Fig. 3c shows the strain-electric field (*S-E*) curve of KNN-BZ ceramics. All samples exhibit standard *S-E* curves with low strain hysteresis. Fig. 3d displays the maximum strain (S_{max}) and inverse piezoelectric coefficient ($d_{33}^* = S_{max}/E_{max}$) as a function of BZ content, indicating that ceramics with NPB exhibit increased S_{max} and d_{33}^* values. When the sample with $x = 0.005$, the maximum values of S_{max} and d_{33}^* are 0.108 % and 720 pm V^{-1}, respectively.

For the ceramic with $x = 0.000$ containing R and T phases, the d_{33} and k_p values are 391 pC N^{-1} and 46 %, respectively (Fig. 3e). The addition of BZ content results in a significant increase in d_{33} and k_p, reaching their maximum for the ceramic with $x = 0.005$ (composed of R-O-T phase), with d_{33} and k_p reaching 585 pC N^{-1} and 62 %, respectively. The introduction of BZ content increases ε_r, reaching the value of 3004 at $x = 0.005$ (Fig. 3f). Meanwhile, all samples maintain a relatively low tan δ of about 0.04. The impedance-frequency resonance spectrum with a high phase angle shown in Fig. 3g, implies a high degree of ordered polarization arrangement in poled KNN-BZ ceramics [35]. These investigations show that the trend of dielectric and electromechanical properties with BZ content are consistent with the classical thermodynamic relationship of $d = k\sqrt{s\varepsilon}$, wherein s represents the elastic compliance constant [36].

In the field of practical electromechanical applications, the ideal piezoceramics are those that offer both large d_{33} and high T_C. However, within perovskite ferroelectrics, there typically exists an inverse relationship between d_{33} and T_C. Fig. 4a summarizes the correlation between d_{33} and T_C across various piezoceramics [20,22,25,37–40]. The overall piezoelectric performance of KNN-BZ ceramics is superior to the general trend of reported KNN-based ceramics. Compared to commercial PZT-5 H ceramics, KNN-BZ ceramics not only maintain comparable d_{33} but also exhibit enhanced T_C. The k is a key factor influencing the bandwidth and sensitivity of piezoelectric transducers [41]. As far as we know, among the current non-textured KNN-based ceramics, KNN-BZ ($x = 0.005$) ceramics have the highest k_p (Fig. 4b) [38,40]. Compared with other KNN-based ceramics reported, KNN-BZ ceramics are more favorable candidates for ultrasonic transducers. In cases involving off-resonance piezoelectric devices, such as energy harvesters, the piezoelectric voltage coefficient ($g = d/\varepsilon$) represents another crucial parameter [42]. This importance is attributed to the fact that the energy density depends on the figure of merit ($d_{33} \times g_{33}$). Fig. 4c shows that KNN-BZ ($x = 0.005$) ceramics exhibit excellent $d_{33} \times g_{33}$ (12.78×10^{-12} m^2 N^{-1}) values, even better than most PZT-based ceramics [27,42]. This indicates that KNN-BZ ceramics have great potential for lead-free energy harvesting applications.

2.4. Mesoscopic domain morphology

In Fig. 5a, piezoelectric force microscopy (PFM) amplitude and phase images reveal variations in the domain structure of KNN-BZ ceramics, particularly in response to changes in BZ content. For ceramics with $x = 0.000$ and $x = 0.001$, irregular lamellar domains with sizes ranging from tens of nanometers to micron-scale can be observed. Such domain configuration is similar to typical lead-based relaxor ferroelectrics with strong local structural heterogeneity [43]. This contrasts significantly

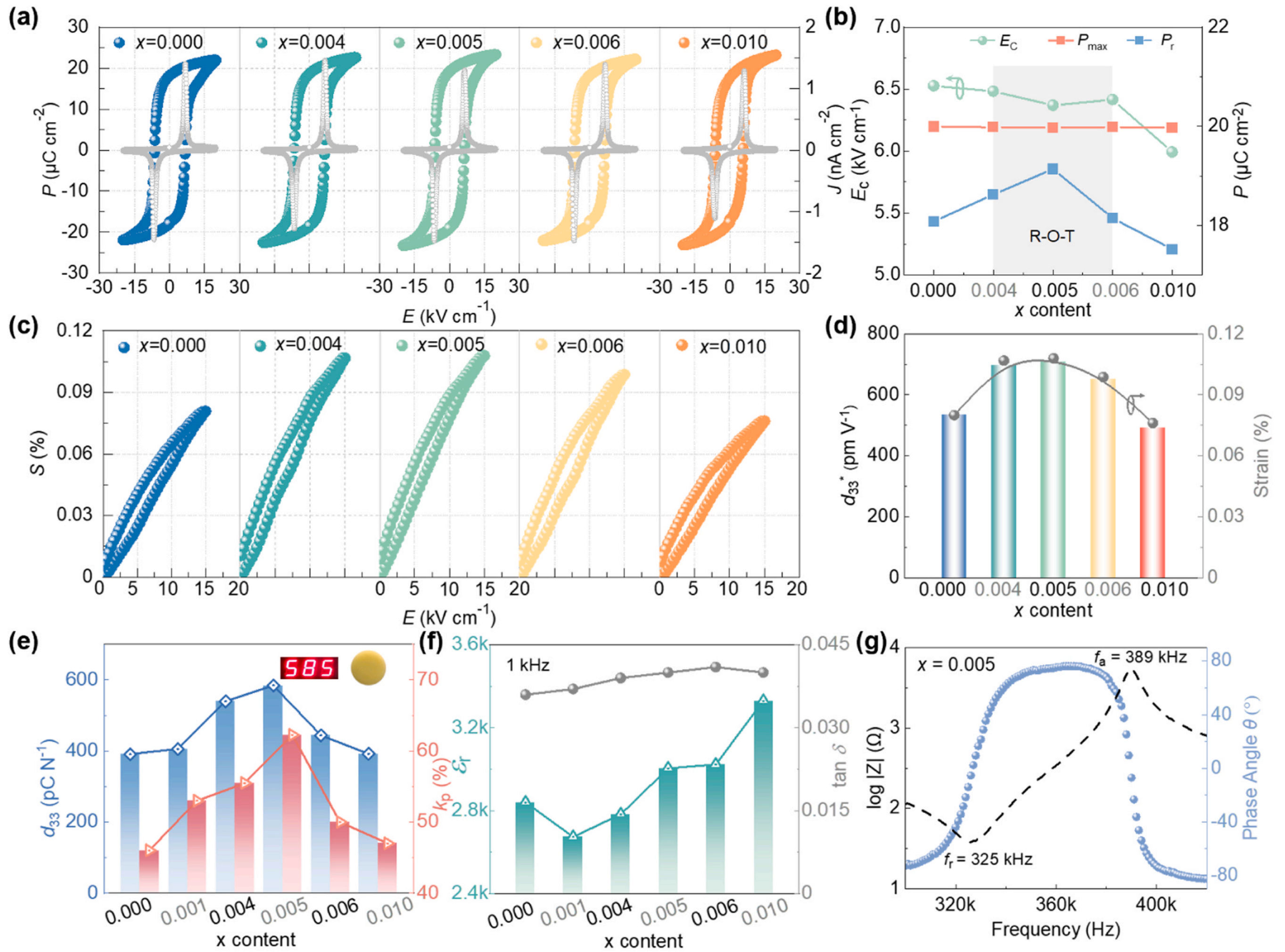

Fig. 3. (a) *P-E* loop and *J-E* curve of KNN-BZ ceramics measured at 1 Hz; the corresponding E_C, P_{max}, and P_r are shown in (b). (c) *S-E* curve of KNN-BZ ceramics measured at 1 Hz; the corresponding d_{33}* and strain are summarized in (d). (e) d_{33} and k_p of KNN-BZ ceramics. (f) ε_r and tanδ of KNN-BZ ceramics. (g) log |Z| and phase angle as a function of frequency for ceramic with x = 0.005.

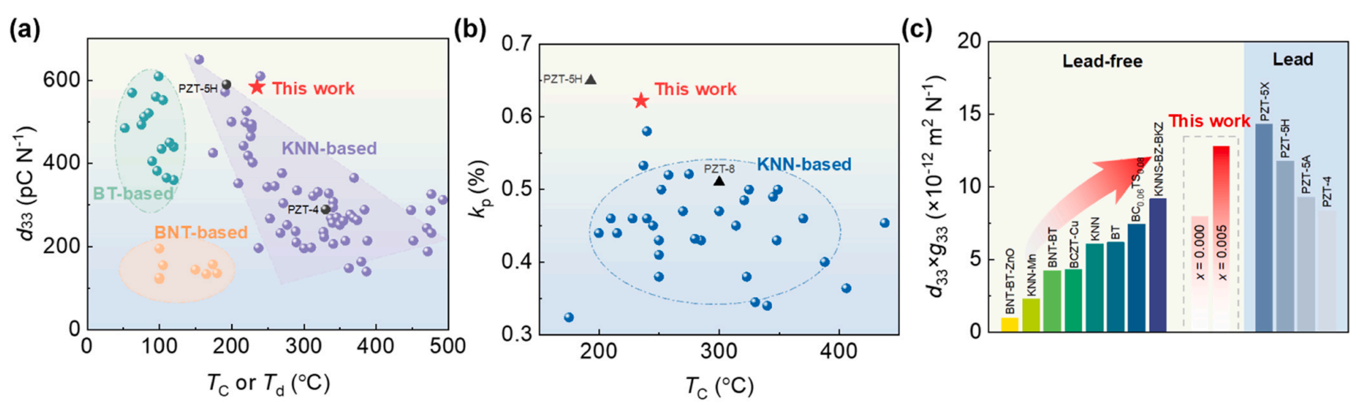

Fig. 4. (a) Comparison of d_{33} and T_C/T_d (T_d: depolarization temperature) in lead-free piezoceramics based on KNN, BNT and BT. (b) Comparison of k_p and T_C in KNN-based piezoceramics. (c) Comparison of d_{33} × g_{33} with representative commercial PZT and lead-free ceramics.

with the domain morphology of pure KNN ceramics, which are defined by large-scale domain structures featuring as "herringbone" and "watermark" patterns [44]. An increase in BZ content to x = 0.004 results in the fragmentation of micron-sized domains into nano-sized domains in ceramics with NPB. Upon increasing the BZ content to x = 0.005, the ceramics uniformly display ultra-small nanodomains. When the BZ content exceeds x = 0.005, there is a gradual reappearance of micro-scale lamellar domains. Obviously, NPB ceramics containing the R-O-T phase have a finer domain structure. This observation is consistent with previous studies of KNN-based ceramics with NPB [21,44]. According to classical theory, a decrease in domain size reduces domain wall energy, which promotes the domain wall motion [45].

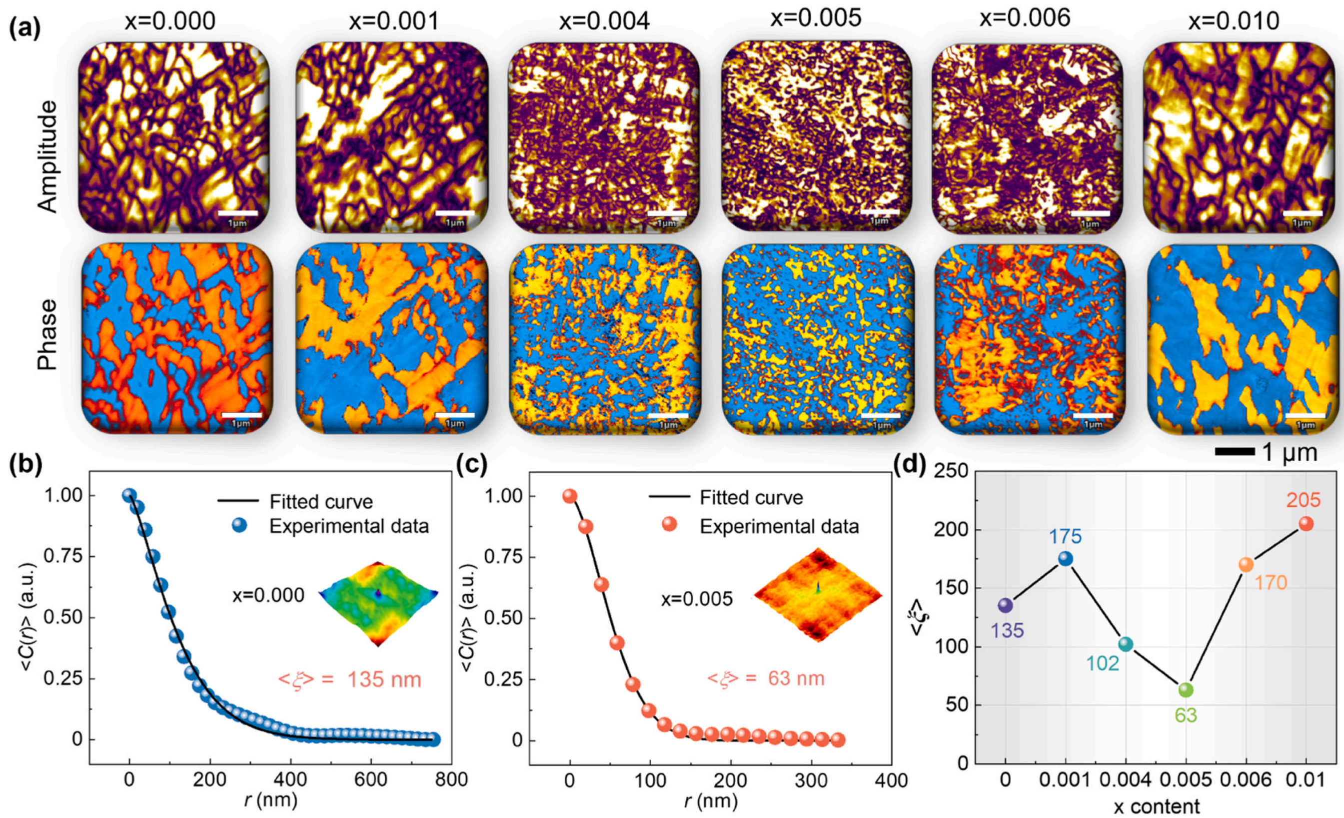

Fig. 5. (a) PFM amplitude and phase images of KNN-BZ ceramics. (b-c) Average autocorrelation function $<C(r)>$ and autocorrelation images of the ceramic with 0.000 and 0.005. (d) The short-range correlation length (ξ) as a function of x content.

Furthermore, these miniaturized domains can effectively reduce the energy barrier during the polarization switching process, acting as "accelerators". The domain size of KNN-BZ ceramics is quantitatively evaluated by the autocorrelation functional method. Parameter $<\xi>$ represents the short-range correlation length, indicating the size of the domain. Autocorrelation images and the corresponding fitting results of KNN-BZ ceramics with $x = 0.000$, 0.001, 0.004, 0.005, 0.006 and 0.010, shown in Fig. 5b-d and Figure S12, determine the average domain sizes $<\xi>$ to be 135, 175, 102, 63, 170 and 205 nm, respectively. The fitting results verify the presence of a finer domain structure in NPB samples with the R-O-T phase.

Based on the research results, NPB-incorporated KNN-BZ ceramics can be classified as "adaptive ferroelectric states". The adaptive state, stemming from multi-domain martensite of metal material, is described as "an adaptive state being constituted of self-assembled microdomains with small domain wall energy, as an outcome to minimize stress induced by structural transitions" [46]. The evolution of this typical martensitic stress-adaptive domain structure also occurs in other displacement transformation [47]. The characteristics of adaptive martensites demonstrate significant potential applicability to KNN-BZ ceramics with NPB. The relationship between structure and properties of ferroelectric domains is established by studying the domain structure: (i) Along with the phase structure changes caused by BZ modification, ferroelectric domains exhibit self-adjusting characteristics; (ii) Self-adjusting miniaturized nanodomains contribute to the excellent electromechanical properties of NPB ceramics.

2.5. Microscopic lattice structure

To explore the potential physical origin of miniaturized domains, Fig. 6a shows the domain structure of ceramic with $x = 0.005$, as characterized by transmission electron microscopy (TEM), revealing a complex, hierarchical arrangement of domains. It includes striped domains with widths of hundreds of nanometers, watermark-like domains with widths of tens of nanometers, and ultra-small nanodomains. Of particular importance, the ultra-small nanodomains play a crucial role in contributing to the DPT around T_C and the superior electromechanical properties of NPB samples. Microscopic high-angle-annular-dark-field (STEM-HAADF) technique can provide detailed information on the local lattice structure and symmetry of ferroelectric materials. According to the theoretical models of respective center atom displacements under various zone axes (Fig. 6d), the disordered polar state composed of R-O-T phase can be identified in Fig. 6b-c. It is evident that the R-O-T phase shows interlocked and disordered lattice distribution, accompanied by a gradual transformation of the polarization vectors, resulting in a "slush nano-polar state" [22]. These nano-polar states constitute the source of ultra-small nanodomains within NPB-incorporated KNN-BZ ceramics. Moreover, disordered lattice distributions usually indicate local structure heterogeneity in multiphase perovskite structure [48,49]. Fig. 6e-g shows the polarization length, normalized intensity of A-site ions, and c/a ratio of unit cells, respectively. Through the visual comparison of these corresponding physical parameters, it is further confirmed that the NPB-incorporated KNN-BZ ceramics have strong local structural heterogeneity. Therefore, the origin of the miniaturized nanodomains in this ceramics can be attributed to strong structural heterogeneity at the nanometer scale.

2.6. Adaptive ferroelectric states and structure-performance relationship

According to classical thermodynamic theory, the formation of stable ferroelectric domains arises from competition and balance among various energies including bulk energy, domain wall energy, electrostatic energy and elastic energy, aiming to minimize the total free energy [43,50]. Based on Geometrical Phase Analysis (GPA), in this case of KNN-BZ ceramics with multiphase structure, the interlocked and disordered lattice distributions may result in lattice mismatch during

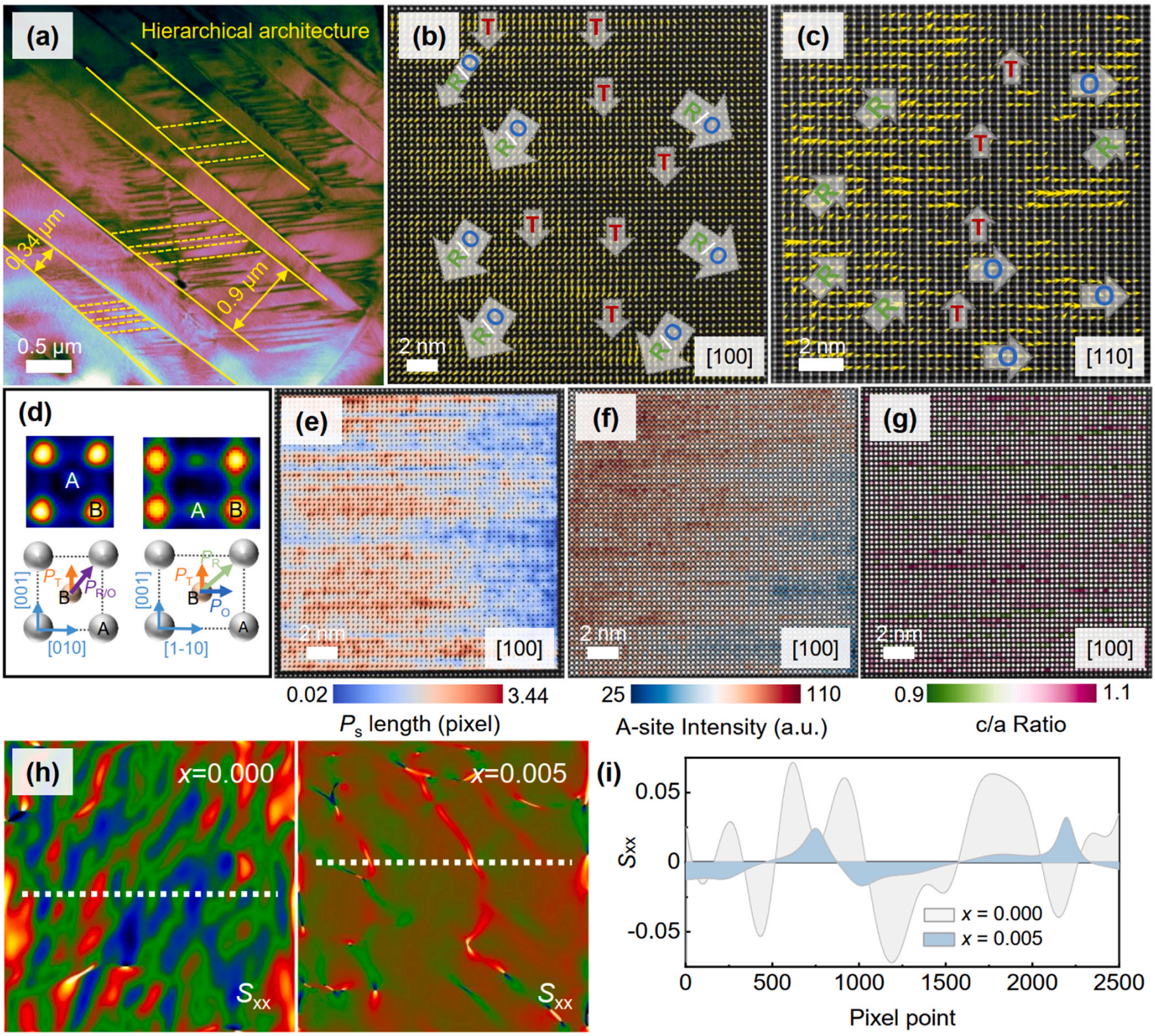

Fig. 6. (a) Bright-field TEM image of domain structures for the ceramic with $x = 0.005$. (b-c) Atomic-resolution polarization vector image. (d) Schematic projection of the unit cell along [100] and [110]. (e) Length of spontaneous polarization (P_s). (f) Normalized intensities of the A-site sublattice. (g) Unit cell c/a ratio. (h) Local strain S_{xx} mapping via GPA. (i) Quantitative S_{xx} analysis of the white dotted lines extracted in (h).

structural transformation, subsequently resulting in the appearance of local stress field, as shown in Fig. 6h. The self-adjusting behavior of the domain structure is the outcome to minimize the local stress fields generated by the lattice mismatch within KNN-BZ ceramics. In Fig. 6i, the quantitative theoretical analysis reveals that the local strain S_{xx} (~2 %) in the ceramic with $x = 0.005$ is significantly lower than in the ceramic with $x = 0.000$ (~7 %), suggesting that the ultra-small nanodomains structure tends to release local stress in KNN-based ceramics. Generally, domain walls, which separate regions of differing polarization directions, play a crucial role in lowering strain and electrostatic energy by inducing adjacent domains to arrange in a “head-to-tail” pattern [46,51]. In response to lattice mismatch induced by local structure heterogeneity, the domains of KNN-BZ ceramics with NPB will self-adjust to form finer nanodomains. These miniaturized domains exhibit lower domain wall energy, following the classical relationship where domain wall energy is proportional to domain size. Based on the analysis of macroscopic electromechanical properties, mesoscopic domain morphology, and microscopic lattice structure, NPB-incorporated KNN-BZ ceramics exhibit excellent electromechanical properties due to the formation of self-adjusting nanodomains in response to strong local structural heterogeneity.

3. Conclusions

In this work, by engineering a "new phase boundary (NPB)" characterized by the R-O-T phase coexistence and refined domain structure, outstanding electromechanical performances (d_{33} ~ 585 pC N^{-1}, k_p ~ 62 %, ε_r ~ 3004, $d_{33} \times g_{33}$ ~ 12.78 $\times 10^{-12}$ $m^2 N^{-1}$ and T_C ~ 235 °C) are obtained in KNN-BZ ceramic. Through systematic analyses of electrical properties, domain morphologies, and lattice structures, our research reveals the origins of the enhanced electromechanical properties in KNN-BZ ceramics with NPB, framing it as "adaptive ferroelectric states", characterized by the formation of self-adjusting nanodomains. The self-adjusting nanodomains and corresponding local structural heterogeneity are formed as an outcome of minimizing the local stress generated by the lattice mismatch within KNN-based ceramics. These insights significantly contribute to understanding the relationship between structure and property in ferroelectrics that incorporate novel phase boundaries.

4. Experimental

Ceramics with the composition (0.96-x)$K_{0.48}Na_{0.52}Nb_{0.96}Sb_{0.04}O_3-0.04Bi_{0.5}Na_{0.5}ZrO_3$-$x$$BaZrO_3$ ($x = 0.000 \sim 0.010$) were synthesized by the solid-state method. High-purity raw materials, including K_2CO_3, Na_2CO_3, Nb_2O_5, Sb_2O_3, Bi_2O_3, ZrO_2 and $BaCO_3$, were selected. These materials were ball-milled in absolute ethanol for 24 h, then the milled slurry was dried at 120 °C and calcined at 850 °C for 6 h. Following a second round of ball milling and drying, the powder was mixed with 7 wt% polyvinyl alcohol and pressed into disks (10 mm diameter; 1 mm thickness) at 10 MPa. The green bodied were then calcined at 750 °C for 2 h to eliminate organic substances and sintered at 1095 °C ~ 1100 °C for 8 h. After sintering, ceramics were polished with Al_2O_3 powders, coated with silver, and heated at 650 °C for 30 min to form Ag electrodes.

The phase structure of the samples was characterized by XRD (Aeris, Malvern Panalytical). The surface structure was examined using scanning electron microscopy (SEM, Quanta 200FEG, FEI). Domain structure was observed using a PFM (MFP-3D, Asylum Research). To determine the relative size of the nanodomains, the average autocorrelation function $<C(r)>$ was calculated using formula $< C(r) > = \sigma^2 \exp[-(r/ < \xi >)^{2b}]$. The short-range correlation length $<\xi>$ was related to the degree of polarization correlation and represents the average relative size of the nanodomains. The variables r and b ($0 < b < 1$) correspond to the distance from any point to the midpoint in the autocorrelation plot and the roughness of the interface at the polarization points, respectively. A higher degree of polarization correlation results in larger domain sizes and more ordered structures. Raman microscopy (HR800, Horiba) with a temperature control system (TMS94, Linkam) was used to obtain the excited Raman spectra at 532 nm. TEM (Talos F200, FEI) was employed to examine the nanoscale structure of the KNN system. For the preparation of the ceramics for STEM-HAADF imaging (Titan G2, FEI), the ceramics underwent mechanical thinning and were subsequently refined by argon ion beam milling. SuperX EDS systems were used to obtain the elemental distribution. To reduce noise, STEM images were processed using Fourier filtering with a lattice mask. The position vector for each unit cell was calculated using two-dimensional Gaussian fitting. This allowed for the determination of the polarization vector, A-site intensity, and the c/a ratio, using specially developed scripts. For electrical property evaluation, the bulk ceramic was poled at 20 kV cm^{-1} in silicone oil for 20 min, followed by a 24 h aging. Dielectric properties of the ceramics were measured using an impedance analyzer (Agilent, E4294 A). The d_{33} was determined by a quasi-static d_{33}-meter (ZJ-4A, Institute of Acoustics). *P-E* loops and *S-E* curves were recorded at 1 Hz using a ferroelectric analyzer (TF Analyzer 2000, aix-ACCT) equipped with a laser interferometer vibrometer (SPeS 120, SIOS).

CRediT authorship contribution statement

Yang Liu: Writing – original draft, Validation, Methodology, Conceptualization. **Xudong Qi:** Writing – original draft, Resources, Investigation, Funding acquisition. **Jinhui Fan:** Software, Resources. **Bingzhong Shen:** Methodology, Investigation, Data curation. **Kui Yao:** Writing – review & editing, Supervision, Funding acquisition, Data curation. **Rui Zhang:** Writing – review & editing, Supervision, Funding acquisition, Data curation.

Declaration of Competing Interest

The authors declare that they have no known competing financial interests or personal relationships that could have appeared to influence the work reported in this paper.

Data availability

Data will be made available on request.

Acknowledgements

This research was financially supported by the National Natural Science Foundation of China (Grant No. 11974093), Heilongjiang Touyan Innovation Team Program (Grant No. XNAUEA5640201720-09), Medical Engineering (Science) cross research fund of Harbin Institute of Technology (Grant No. IR2021238), Open Project Program of Guangdong Provincial Key Laboratory of Electronic Functional Materials and Devices (Grant No. EFMD2022006Z). The author from IMRE acknowledges partial supports from A*STAR, under RIE2020 AME Programmatic Fund (Grant No. A20G9b0135), Singapore. Thanks to Dr. K. Li for the help of PFM measurement.

Appendix A. Supporting information

Supplementary data associated with this article can be found in the online version at doi:10.1016/j.nanoen.2024.109972.

References

[1] E. Sun, W. Cao, Relaxor-based ferroelectric single crystals: growth, domain engineering, characterization and applications, Prog. Mater. Sci. 65 (2014) 124–210.
[2] M. Waqar, H. Wu, J. Chen, K. Yao, J. Wang, Evolution from lead-based to lead-free piezoelectrics: engineering of lattices, domains, boundaries, and defects leading to giant response, Adv. Mater. 34 (2022) 2106845.
[3] S. Dong, Review on piezoelectric, ultrasonic, and magnetoelectric actuators, J. Adv. Dielectr. 02 (2012) 1230001.
[4] L. Chen, H. Liu, H. Qi, J. Chen, High-electromechanical performance for high-power piezoelectric applications: Fundamental, progress, and perspective, Prog. Mater. Sci. 127 (2022) 100944.
[5] J. Li, W. Qu, J. Daniels, H. Wu, L. Liu, J. Wu, M. Wang, S. Checchia, S. Yang, H. Lei, R. Lv, Y. Zhang, D. Wang, X. Li, X. Ding, J. Sun, Z. Xu, Y. Chang, S. Zhang, F. Li, Lead zirconate titanate ceramics with aligned crystallite grains, Science 380 (2023) 87.
[6] T. Shrout, S. Zhang, Lead-free piezoelectric ceramics: alternatives for PZT? J. Electroceram. 19 (2007) 113–126.
[7] S. Zhang, B. Malič, J. Li, J. Rödel, Lead-free ferroelectric materials: prospective applications, J. Mater. Res. 36 (2021) 985–995.
[8] M. Lee, D. Kim, J. Park, S. Kim, T. Song, M. Kim, W. Kim, D. Do, I. Jeong, High-performance lead-free piezoceramics with high curie temperatures, Adv. Mater. 27 (2015) 6976–6982.
[9] W. Liu, X. Ren, Large piezoelectric effect in Pb-free ceramics, Phys. Rev. Lett. 103 (2009) 257602.
[10] X. Liu, X. Tan, Giant strains in non-textured $(Bi_{1/2}Na_{1/2})TiO_3$-based lead-free ceramics, Adv. Mater. 28 (2016) 574–578.
[11] Y. Saito, H. Takao, T. Tani, T. Nonoyama, K. Takatori, T. Homma, T. Nagaya, M. Nakamura, Lead-free piezoceramics, Nature 432 (2004) 84–87.
[12] X. Wang, J. Wu, D. Xiao, J. Zhu, X. Cheng, T. Zheng, B. Zhang, X. Lou, X. Wang, Giant piezoelectricity in potassium-sodium niobate lead-free ceramics, J. Am. Chem. Soc. 136 (2014) 2905–2910.
[13] Y. Liu, B. Shen, L. Bian, J. Hao, B. Yang, R. Zhang, W. Cao, Enhanced electromechanical performance in lead-free $(Na,K)NbO_3$-based piezoceramics via the synergistic design of texture engineering and Sm-modification, ACS Appl. Mater. Interfaces 15 (2023) 47221–47228.
[14] Z. Cen, Y. Huan, W. Feng, Y. Yu, P. Zhao, L. Chen, C. Zhu, L. Li, X. Wang, A high temperature stable piezoelectric strain of KNN-based ceramics, J. Mater. Chem. A 6 (2018) 19967–19973.
[15] T. Zheng, Y. Yu, H. Lei, F. Li, S. Zhang, J. Zhu, J. Wu, Compositionally graded KNN-based multilayer composite with excellent piezoelectric temperature stability, Adv. Mater. 34 (2022) 2109175.
[16] J. Lin, G. Ge, J. Li, J. Qian, K. Zhu, Y. Wei, C. Shi, G. Li, F. Yan, W. Li, J. Zhang, J. Zhai, H. Wu, Field-induced multiscale polarization configuration transitions of mesentropic lead-free piezoceramics achieving giant energy harvesting performance, Adv. Funct. Mater. 33 (2023) 2303965.
[17] G. Huangfu, K. Zeng, B. Wang, J. Wang, Z. Fu, F. Xu, S. Zhang, H. Luo, D. Viehland, Y. Guo, Giant electric field-induced strain in lead-free piezoceramics, Science 378 (2023) 1125–1130.
[18] F. Yao, K. Wang, W. Jo, K. Webber, T. Comyn, J. Ding, B. Xu, L. Cheng, M. Zheng, Y. Hou, J. Li, Diffused phase transition boosts thermal stability of high-performance lead-free piezoelectrics, Adv. Funct. Mater. 26 (2016) 1217–1224.

[19] H. Wu, Y. Zhang, J. Wu, J. Wang, S. Pennycook, Microstructural origins of high piezoelectric performance: a pathway to practical lead-free materials, Adv. Funct. Mater. 29 (2019) 1902911.
[20] Q. Liu, Y. Zhang, J. Gao, Z. Zhou, D. Yang, K. Lee, A. Studer, M. Hinterstein, K. Wang, X. Zhang, L. Li, J. Li, Practical high-performance lead-free piezoelectrics: structural flexibility beyond utilizing multiphase coexistence, Natl. Sci. Rev. 7 (2020) 355–365.
[21] X. Lv, J. Zhu, D. Xiao, X. Zhang, J. Wu, Emerging new phase boundary in potassium sodium-niobate based ceramics, Chem. Soc. Rev. 49 (2020) 671–707.
[22] H. Tao, H. Wu, Y. Liu, Y. Zhang, J. Wu, F. Li, X. Lyu, C. Zhao, D. Xiao, J. Zhu, S. Pennycook, Ultrahigh performance in lead-free piezoceramics utilizing a relaxor slush polar state with multiphase coexistence, J. Am. Chem. Soc. 141 (2019) 13987–13994.
[23] H. Thong, Z. Li, J. Lu, C. Li, Y. Liu, Q. Sun, Z. Fu, Y. Wei, K. Wang, Domain engineering in bulk ferroelectric ceramics via mesoscopic chemical inhomogeneity, Adv. Sci. 9 (2022) 2200998.
[24] Z. Tan, J. Xing, Y. Peng, Q. Zhang, J. Zhu, Polarization rotation boosts strong piezoelectric response in the lead-free perovskite ferroelectric $K_{0.5}Na_{0.5}NbO_3$, Phys. Rev. B 104 (2021) 014104.
[25] C. Zhou, J. Zhang, W. Yao, D. Liu, G. He, Remarkably strong piezoelectricity, rhombohedral-orthorhombic-tetragonal phase coexistence and domain structure of $(K,Na)(Nb,Sb)O_3$-$(Bi,Na)ZrO_3$-$BaZrO_3$ ceramics, J. Alloy Compd. 820 (2020) 153411.
[26] Y. Huan, T. Wei, Z. Wang, C. Lei, F. Chen, X. Wang, Polarization switching and rotation in KNN-based lead-free piezoelectric ceramics near the polymorphic phase boundary, J. Eur. Ceram. Soc. 39 (2019) 1002–1010.
[27] K. Xi, Y. Hou, M. Zheng, M. Zhu, Elastic polarization configuration coupled with activity rattling space boosts energy harvesting performance of lead-free piezoceramic, Adv. Funct. Mater. 202401487 (2024).
[28] J. Wang, L. Luo, Y. Huang, W. Li, J. Varela, Effect of Yb codoping on the phase transition, and electrical and photoluminescence properties in KNLN:Er/xYb ceramics, J. Am. Ceram. Soc. 99 (2016) 1625–1630.
[29] X. Lv, J. Wu, X. Zhang, Reduced degree of phase coexistence in KNN-Based ceramics by competing additives, J. Eur. Ceram. Soc. 40 (2020) 2945–2953.
[30] T. Zheng, Y. Zhang, Q. Ke, H. Wu, L.W. Heng, D. Xiao, J. Zhu, S. Pennycook, K. Yao, J. Wu, High-performance potassium sodium niobate piezoceramics for ultrasonic transducer, Nano Energy 70 (2020) 104559.
[31] M. Zhang, K. Wang, Y. Du, G. Dai, W. Sun, G. Li, D. Hu, H. Thong, C. Zhao, X. Xi, Z. Yue, J. Li, High and temperature-insensitive piezoelectric strain in alkali niobate lead-free perovskite, J. Am. Chem. Soc. 139 (2017) 3889–3895.
[32] R. Li, X. Sun, X. Lv, T. Zheng, J. Wu, Manipulating temperature stability in KNN-based ceramics via defect design, Acta Mater. 218 (2021) 117229.
[33] X. Huang, W. Li, J. Zeng, L. Zheng, Z. Man, G. Li, The grain size effect in dielectric diffusion and electrical conduction of PZnTe-PZT ceramics, Phys. B 560 (2019) 16–22.
[34] Y. Liu, B. Shen, J. Fan, X. Qi, E. Sun, R. Zhang, Dynamic hysteresis relation for guiding poling condition of high-performance KNN-based ceramics, J. Eur. Ceram. Soc. 43 (2023) 4044–4050.
[35] Y. Liu, W. Qu, H. Thong, Y. Zhang, Y. Zhang, F. ZYao, T. Nguyen, J. Li, M. Zhang, J. Li, B. Han, W. Gong, H. Wu, C. Wu, B. Xu, K. Wang, Isolated-oxygen-vacancy hardening in lead-free piezoelectrics, Adv. Mater. 34 (2022) 2202558.
[36] F. Li, S. Zhang, Z. Xu, X. Wei, T. Shrout, Critical property in relaxor-$PbTiO_3$ single crystals-shear piezoelectric response, Adv. Funct. Mater. 21 (2011) 2118–2128.
[37] Y. Zhang, J. Li, Review of chemical modification on potassium sodium niobate lead-free piezoelectrics, J. Mater. Chem. C 7 (2019) 4284–4303.
[38] J. Xing, T. Zheng, J. Wu, D. Xiao, J. Zhu, Progress on the doping and phase boundary design of potassium-sodium niobate lead-free ceramics, J. Adv. Dielectr. 08 (2018) 18300037.
[39] J. Rödel, K. Webber, R. Dittmer, W. Jo, M. Kimura, D. Damjanovic, Transferring lead-free piezoelectric ceramics into application, J. Eur. Ceram. Soc. 35 (2015) 1659–1681.
[40] C. Sherman, J. Butler, Transducers and Arrays for Underwater Sound, Springer, New York, 2007.
[41] Y. Liu, K. Zhu, B. Shen, J. Ma, L. Bian, R. Zhang, W. Cao, Broadband ultrasonic transducer based on textured lead-free NKN-based piezoceramics, Ceram. Int. 49 (2023) 40450–40456.
[42] Y. Sun, Y. Chang, J. Wu, Y. Liu, L. Jin, S. Zhang, B. Yang, W. Cao, Ultrahigh energy harvesting properties in textured lead-free piezoelectric composites, J. Mater. Chem. A 7 (2019) 3603–3611.
[43] F. Li, D. Lin, Z. Chen, Z. Cheng, J. Wang, C. Li, Z. Xu, Q. Huang, X. Liao, L. Chen, T. Shrout, S. Zhang, Ultrahigh piezoelectricity in ferroelectric ceramics by design, Nat. Mater. 17 (2018) 349–354.
[44] X. Lv, X. Zhang, J. Wu, Nano-domains in lead-free piezoceramics: a review, J. Mater. Chem. A 8 (2020) 10026–10073.
[45] P. Li, J. Zhai, B. Shen, S. Zhang, X. Li, F. Zhu, X. Zhang, Ultrahigh piezoelectric properties in textured $(K,Na)NbO_3$-based lead-free ceramics, Adv. Mater. 30 (2018) 1705171.
[46] Y. Jin, Y. Wang, A. Khachaturyan, J. Li, D. Viehland, Adaptive ferroelectric states in systems with low domain wall energy: tetragonal microdomains, J. Appl. Phys. 94 (2003) 3629–3640.
[47] Y. Jin, Y. Wang, A. Khachaturyan, J. Li, D. Viehland, Conformal miniaturization of domains with low domain-wall energy: Monoclinic ferroelectric states near the morphotropic phase boundaries, Phys. Rev. Lett. 91 (2003) 197601.
[48] H. Liu, X. Shi, Y. Yao, H. Luo, Q. Li, H. Huang, H. Qi, Y. Zhang, Y. Ren, S. Kelly, K. Roleder, J. Neuefeind, L. Chen, X. Xing, J. Chen, Emergence of high piezoelectricity from competing local polar order-disorder in relaxor ferroelectrics, Nat. Commun. 14 (2023) 1007.
[49] M. Zhang, S. Lan, B. Bing, H. Pan, Y. Liu, Q. Zhang, J. Qi, D. Chen, H. Su, D. Yi, Y. Yang, R. Wei, H. Cai, H. Han, L. Gu, C. Nan, Y. Lin, Ultrahigh energy storage in high-entropy ceramic capacitors with polymorphic relaxor phase, Science 384 (2024) 185–189.
[50] J. Yin, H. Zong, H. Tao, X. Tao, H. Wu, Y. Zhang, L. Zhao, X. Ding, J. Sun, J. Zhu, J. Wu, S. Pennycook, Nanoscale bubble domains with polar topologies in bulk ferroelectrics, Nat. Commun. 12 (2021) 3632.
[51] J. Lin, J. Qian, G. Ge, Y. Yang, J. Li, X. Wu, G. Li, S. Wang, Y. Liu, J. Zhang, J. Zhai, X. Shi, H. Wu, Multiscale reconfiguration induced highly saturated poling in lead-free piezoceramics for giant energy conversion, Nat. Commun. 15 (2024) 2560.

Yang Liu is a Ph.D. candidate in the School of Instrumentation Science and Engineering, Harbin Institute of Technology. He is currently a joint-training Ph.D. student at Institute of Materials Research and Engineering (IMRE), Agency for Science, Technology and Research (A*STAR) in Singapore. His research focuses on the design and fabrication of KNN-based lead-free piezoceramics and ultrasonic transducers.

Jinhui Fan is a Ph.D. candidate in the School of Instrumentation Science and Engineering, Harbin Institute of Technology. His research interests focus on ferroelectric single crystals and its structure-property relationship.

Xudong Qi received his Ph.D. in Physics from Harbin Institute of Technology in 2019. His research focuses on the structure-property relationships and device applications of high-performance ferroelectric single crystals and ceramics.

Bingzhong Shen received his Ph.D. from the School of Instrumentation Science and Engineering at Harbin Institute of Technology in 2024. His research interests include the preparation of piezoelectric, ferroelectric, and antiferroelectric materials, as well as the regulation of their piezoelectric, energy storage, and electrocaloric properties.

Rui Zhang received his Ph.D. in Biomedical Engineering from Xi'an Jiaotong University, China, in 2000. He is currently a professor at Harbin Institute of Technology. He is also a senior member of the Chinese Association of Ultrasound in Medicine and Engineering, a member of the American Society for Materials, and the American Society of Electrical and Electronic Engineers. His research interests include ultrasonic electronics, acoustic functional material, ultrasonic image processing and the development of acousto-optic diagnosis and treatment equipment.

Kui Yao is a Senior Principal Scientist at the Institute of Materials Research and Engineering (IMRE), Agency for Science, Technology and Research (A*STAR), Singapore. His research areas cover dielectric, piezoelectric, and ferroelectric materials, and the sensors and transducers enabled by these materials, including their applications for structural and condition monitoring, ultrasonic and photoacoustic detection and diagnosis, noise and vibration mitigation.